Mass Preserving Image Registration: Results of Evaluation of Methods for Pulmonary Image Registration 2010 Challenge

Vladlena Gorbunova[1], Jon Sporring[1], Pechin Lo[1], Asger Dirksen[3], and Marleen de Bruijne[1,2]

[1] Department of Computer Science, University of Copenhagen, Denmark
[2] Biomedical Imaging Group Rotterdam, Erasmus MC, Rotterdam, the Netherlands
[3] Department of Respiratory Medicine, Gentofte University Hospital, Denmark

Abstract. The paper presents results the mass preserving image registration method in the Evaluation of Methods for Pulmonary Image Registration 2010 (EMPIRE10) Challenge. The mass preserving image registration algorithm was applied to the 20 image pairs. Registration was evaluated using four different scores: lung boundary alignment, major fissure alignment, landmark alignment and transform singularity scores. The registration algorithm achieved an average landmark alignment score of 2.20 ± 2.05 mm and the median of 1.29 mm. In 19 out of 20 image pairs, the method produced invertible deformations. Overall, the mass preserving image registration method was ranked 20th out of 34 participants.

1 Introduction

Registration of lung CT images is increasingly used in various research topics. Three main applications may be distinguished as follows [1] : atlas registration based segmentation of the lungs and structures within the lungs; registration of longitudinal CT image series to monitor disease progression; registration of successive frames in dynamic CT sequences to estimate local ventilation and perfusion.

For intra-subject registration of lung CT images, which is the case in this challenge, SSD is probably the most commonly used similarity measure. Sum of squared differences is optimal when corresponding anatomical points are represented by the same intensity in the images, with additional Gaussian noise. This is a valid assumption because Hounsfield unit (HU) in CT scan represents the density of tissue. Densities of the same tissue is often expected to remain constant in different scans. Previous studies on lung CT scans showed that density of lung tissue depends on regional ventilation and changes during breathing [2, 3]. The basic assumption of SSD similarity function does not hold for lung tissue and as a possible solution we propose to model appearance of lung tissue in CT scan with respect to the regional ventilation using a simple law of mass preservation.

In the mass preserving model, density of the lung tissue is inverse proportional to the local volume. Therefore change in local volume could be computed from the change in the density. First, Simon et al. [4] proposed this model and applied it to estimate regional ventilation from image intensity in 4D-CT lung scans. Vice versa, the change in density of the lung tissue could be computed from the change in the local volume. Under applied local deformations the density of the lung tissue is directly proportional to the determinant of the Jacobian of the transform function, associated with the deformations. Recently, Reinhardt et al. [5] showed strong correlation between regional ventilation obtained from the Xe-CT image and the ventilation computed from the image registration procedure. In the latter case, regional ventilation was computed from the determinant of Jacobian of the obtained transformation between the two images.

Several recent studies have incorporated mass preserving assumption in registration process. Sarrut et al. [3] proposed to modify lung density in a 4D-CT image prior to registration. Tannenbaum et al. [6] proposed a completely new registration method which establishes the optimal mass transportation between the images while the image intensities remain constant. Castillo et al. [7] proposed to incorporate the mass preserving intensity modification model into the optical-flow registration and applied it to the 4D-CT images.

We developed our registration method based on the results from [5] and modeled the lung tissue density using the determinant of the Jacobian of the transform function. We modified the sum of squared differences similarity function to enable mass preservation and continuously simulated the appearance of the lung tissue under the given deformations.

This work was presented in [8, 9]. Since then a similar idea has been used by Yin et al. [10, 11], where the mass preserving image registration was applied to breath-hold lung CT images acquired at the maximum inspiration and maximum expiration in the same scanning session. We previously applied mass preserving algorithm to the pairs of maximum inspiration and maximum expiration CT scans taken on the same day [9] and to the longitudinal CT scans acquired at maximum inspiration breathhold [8].

2 Mass Preserving Image Registration

This section briefly presents a general deformable image registration framework based on B-Splines which is used in many medical imaging tasks [12, 13], and explains how the proposed mass preserving methodology can be incorporated in this framework.

2.1 Preprocessing

To improve registration performance, segmentations of the lung fields are obtained using region growing and morphological smoothing [14]. Previously, several papers showed better performance of registration if the rib cage was erased from the images [15, 16]. To remove the influence of the rib cage, we extract the

lung area from the images and set the background to 0HU. Finally, the image intensities are shifted with a value 1000HU so that the new intensities approximate the real densities of the tissues.

2.2 Transformation

We follow a common approach and use a multi-resolution image registration strategy. First, the images are registered affinely. To provide an accurate initialization of the affine transform, the trachea and main bronchi are first extracted using a modified fast marching algorithm [17]. The center of the affine transform is then set at the carina point in the fixed image and the initial translation is set to the difference between the carina points in moving and fixed images. Secondly, a series of B-Spline transforms, with corresponding Gaussian smoothing at the coarser levels, is applied to the pre-aligned images. The final transform is thus a composition of a global affine transform T_A and N levels of B-Spline transforms $T^i_{\text{B-Spline}}$ with decreasing grid size:

$$T_{\text{final}}(\mathbf{x}) = T^N_{\text{B-Spline}} \circ ... \circ T^1_{\text{B-Spline}} \circ T_A(\mathbf{x}), \tag{1}$$

where $\mathbf{x} = (x_1, x_2, x_3)$ is a point in the fixed image domain Ω_f.

In this work, we have used small step size along the gradient and multi-level B-Spline grid to ensure that the transform is invertible [18].

2.3 Mass Preserving Similarity Function

We use the sum of squared differences similarity function as the basis for the mass preserving similarity measure,

$$C(I_f, I_m \circ T) = \frac{1}{|\Omega_f|} ||I_f(\mathbf{x}) - I_m(T(\mathbf{x}))||^2_{L_2}, \tag{2}$$

where $\mathbf{x}$ is a point in the region Ω_f occupied by the fixed image I_f, $\mathbf{y} = T(\mathbf{x})$ is the corresponding point in the region Ω_m occupied by the moving image I_m.

The sum of squared differences is an optimal similarity measure if image intensities are identical or differ with Gaussian noise. This assumption does not hold in case of lung CT images, where both blood and air enter the lungs during inhalation. We used a hypothesis that majority of incoming blood stays in the larger vessels, and only air is inhaled into the alveoli. Therefore we can presume that mass of parenchyma remains constant and the density of lung tissue is inverse proportional to the amount of air. Under the applied local deformations, the induced change in local volume is defined by the determinant of Jacobain of the associated transform function.

Using the mass preserving assumption, the intensity of the moving image I_m in a point $\mathbf{y} \in \Omega_M$ is inverse proportional to the change in local volume $\frac{1}{det(J_{T^{-1}})}$ in the point $\mathbf{y}$. The modeled intensity can be written $\hat{I}_m(\mathbf{y}) =$

$[det(J_{T^{-1}}(\mathbf{y}))]^{-1} I_m(\mathbf{y})$. Assuming that the transform function T is invertible, the determinant of Jacobian $J_{T^{-1}}(\mathbf{y})$ is the inverse of the determinant of Jacobian $J_T(\mathbf{x})$ and the modeled intensity of the moving image can be written $\hat{I}_m(\mathbf{y}) = det(J_T(\mathbf{x})) \cdot I_m(\mathbf{y})$.

Finally, the mass preserving intensity model can be naturally incorporated in the standard sum of square differences similarity function:

$$C(I_f, I_m \circ T) = \frac{1}{|\Omega_f|} \int_{\Omega_f} [I_f(\mathbf{x}) - det\left(J_T(\mathbf{x})\right) \cdot I_m(T(\mathbf{x}))]^2 d\mathbf{x}. \tag{3}$$

2.4 Optimization

In this chapter we use a stochastic gradient descent method [19] to optimize the similarity function. The closed form expression for the gradient of the proposed mass preserving similarity function (3) is,

$$\mathcal{D}_{\mathbf{a}} C = -\frac{2}{|\Omega_f|} \int_{\Omega_f} [I_f(\mathbf{x}) - det(J_T(\mathbf{x})) \cdot I_m(T(\mathbf{x}))] \cdot det(J_T(\mathbf{x})) \cdot \tag{4}$$

$$\cdot \left[\mathrm{vec}(J^{-T}(\mathbf{x}))^T \cdot \mathcal{D}_{\mathbf{a}} \mathrm{vec}(J(\mathbf{x})) \cdot I_m(T(\mathbf{x})) - \mathcal{D}_{\mathbf{y}} I_m(T(\mathbf{x})) \cdot \mathcal{D}_{\mathbf{a}} T(\mathbf{x})\right] d\mathbf{x},$$

where $\mathcal{D}_{\mathbf{a}}$ represents a gradient row vector operator with respect to the transform parameters $\mathbf{a}$, $\mathcal{D}_{\mathbf{y}}$ represents a spatial gradient vector operator, and $vec(\cdot)$ is the vector constructed by concatenating all columns of a matrix.

In case of SSD similarity function, only voxels with non-zero image gradient contribute to the gradient thus resulting in a higher uncertainty of registration in homogeneous regions [20]. On the contrary, for the proposed mass preserving similarity function of (4), voxels where the image gradient $\mathcal{D}_{\mathbf{y}} I_m(\mathbf{y})$ is close to zero also contribute to gradient thus providing additional information in homogeneous regions.

3 Experiments

3.1 Preprocessing

Airway trees were segmented using the algorithm as in [21]. For two scan pairs (4 and 10) we provided seed points for the segmentation algorithm manually, because these scan pairs were acquired from sheep and had different airway tree anatomy. The main anatomical difference between human and sheep airways is the tracheal bronchus which branches off from trachea before the carina point. The tracheal bronchus occurs very rare for humans whereas for sheep it is common. Since the airway tree segmentation algorithm from [21] was developed for segmenting human airway tree, the segmentation of sheep airways were corrected manually. The seed point of the algorithm was provided below the branch point of the tracheal bronchus thus disregarding the above part of the airway tree and leading to the correct labelling of the right and left main bronchus.

3.2 Image Registration Setup

We applied three levels of B-Spline transforms, $N = 3$, with decreasing grid size. The first two levels were applied to the deformed moving image blurred Gaussian $\sigma_{1,2} = 1$ voxel and sampled by a factor of two in each direction. The third level was applied to the full resolution image without smoothing. The number of grid cells at first B-Spline level was $3 \times 3 \times 3$ (corresponds to approx. $9.7 \times 7.3 \times 9.3$ cm^3); at the second B-Spline level was $6 \times 6 \times 6$ (corresponds to approx. $4.9 \times 3.6 \times 4.6$ cm^3); at the third B-Spline level was $12 \times 12 \times 12$ (corresponds to approx. $2.4 \times 1.8 \times 2.3$ cm^3). Optimal parameters were obtained by minimizing the cost function between the fixed and the corresponding moving images.

After each level of transform we computed the current deformation field as the sum of the deformation fields from the previous transforms. The original moving image was then deformed with the obtained deformation field and adjusted with respect to the mass preserving model. The Jacobian of the transform was computed using a first order difference scheme with the step equal to the image spacing.

Each of the four transforms in (1) was optimized separately using the stochastic gradient descent [19]. The number of voxel samples was chosen proportional to the number of parameters to optimize, and was set to 50000 for the finest B-Spline transform and to 10000 for the intermediate B-Spline and Affine transforms. Maximum number of iterations was 1000 for all the transforms. The maximum step length along the normalized gradient direction was set to 0.5 mm.

4 Results

Registration was applied to a set of 20 image pairs where each pair was obtained from the same subject. Two image pairs were sheep chest CT scans, the remaining 18 were human lung CT scans. Dataset included images acquired from different phases of 4D-CT and 3D scans, images acquired at maximum inspiration and maximum expiration breathholds. Subjects with severe lung disease as well as relatively healthy subjects were included into the study. In-plane spacing varied from 0.4688×0.4688 mm to 0.9766×0.9766 mm, and slice thickness varied from 0.6 mm to 2.5 mm. Lung masks were provided along with the image pairs by challenge organizers.

Table 1 presents overall evaluation scores averaged over both left and right lung regions. Elaborate results for each evaluation score are reported in tables on the web-page **http://empire10.isi.uu.nl/res_diku.php**, including scores computed in only the left or the right lung regions, in the upper or the lower regions of both lungs or over both the right and the left lung regions. Additionally, the minimum, maximum and average values of landmark alignment score and average distance in anterior-posterior (AR), superior-inferior (SI) and left-right (LR) directions are reported.

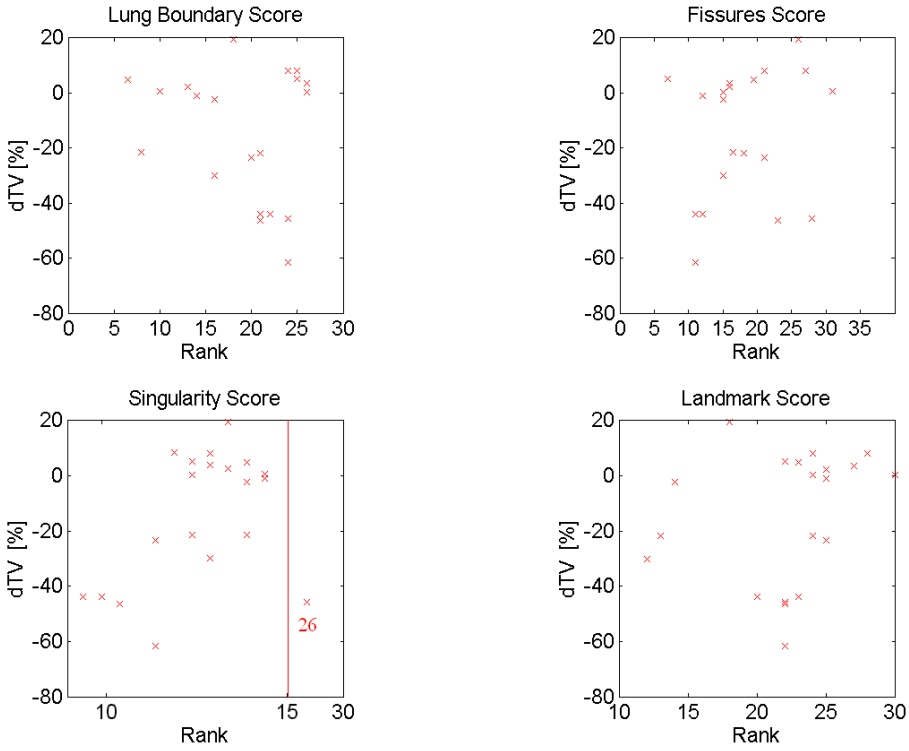

Fig. 1. Each subplot shows overall rank versus the relative lung volume difference.

	Lung Boundaries		Fissures		Landmarks		Singularities	
Scan Pair	**Score**	**Rank**	**Score**	**Rank**	**Score**	**Rank**	**Score**	**Rank**
01	0.22	24.00	0.04	11.00	5.19	22.00	0.00	11.50
02	0.00	26.00	0.00	15.00	0.61	24.00	0.00	12.50
03	0.00	24.00	0.00	27.00	0.75	28.00	0.00	12.00
04	0.00	8.00	0.00	16.50	1.10	13.00	0.00	14.00
05	0.00	13.00	0.00	16.00	0.34	25.00	0.00	13.50
06	0.00	16.00	0.00	15.00	0.35	14.00	0.00	14.00
07	0.21	22.00	0.75	11.00	5.08	23.00	0.00	10.00
08	0.02	21.00	0.08	18.00	1.88	24.00	0.00	12.50
09	0.00	26.00	0.00	16.00	0.94	27.00	0.00	13.00
10	0.00	17.00	0.00	15.00	1.56	13.00	0.00	13.50
11	0.08	20.00	0.26	21.00	2.27	25.00	0.00	11.50
12	0.00	10.00	0.03	31.00	1.31	30.00	0.00	14.50
13	0.00	25.00	0.11	21.00	1.26	24.00	0.00	13.00
14	0.16	21.00	3.01	12.00	5.42	20.00	0.00	9.50
15	0.00	25.00	0.00	7.00	0.77	22.00	0.00	12.50
16	0.00	18.00	0.40	26.00	1.33	18.00	0.00	13.50
17	0.00	6.50	0.05	19.50	1.16	23.00	0.00	14.00
18	0.09	21.00	5.10	23.00	5.14	22.00	0.00	10.50
19	0.00	14.00	0.00	12.00	0.64	25.00	0.00	14.50
20	0.12	24.00	9.90	28.00	6.75	22.00	0.01	26.00
Avg	0.04	19.07	0.99	18.04	2.19	22.20	0.00	13.30
Average Ranking Overall								18.15
Final Placement								20

Table 1. Results for each scan pair, per category and overall. Rankings and final placement are from a total of 34 competing algorithms.

Figure 1 displays relationship between the ranking of the mass preserving registration and the relative lung volume difference between the fixed and the moving images. Correlation of the relative lung volume difference with the landmark alignment score was -0.87 ($p < 10^{-6}$); with the lung boundary alignment score was -0.85 ($p < 10^{-5}$); with the fissure alignment score was -0.52 ($p = 0.02$); and with the singularity score $= 0.31$ ($p = 0.18$).

In order to investigate spatial properties of the mass preserving registration method, we performed Student's t-test between the scores for the right and the left lung regions, between the scores for the top and the bottom regions of both lungs and between the three spatial directions AP, SI and LR. The following scores differ significantly:

– Alignment of the upper part of lung boundaries 0.0033% is significantly better than the alignment of the lower part of lung boundaries 0.0826%, the corresponding p-value 0.014;
– Landmark alignment in the upper part 1.92 mm is significantly smaller than landmark alignment in the lower part 2.49 mm, $p = 0.030$;
– Landmark alignment in the LR direction 0.75 mm is significantly smaller than both alignment in AP 1.24 mm and SI 1.13 mm directions, with the corresponding p-values 0.0034 and 0.0097 respectively.

Running time of the optimisation process for all four transforms was on average 1 hour and 52 minutes and ranged from 48 minutes to 2 hours and 56 minutes. The additional time required for resampling the moving image, loading or saving images is not included into the reported time because it depends drastically on the image size.

5 Discussion

Data analysis showed clear asymmetry in the fixed and the moving images. Lung CT scan with smaller lung volume in the image pair were usually set as the fixed image in the registration framework. The relative volume difference between the lungs of the fixed and the moving images was on average $\Delta\text{TV} = 100 \cdot \frac{V_f - V_m}{(V_f + V_m)/2} = -14.47\%$. This potentially leads to a more difficult registration problem than if the image with the bigger lung volume is chosen as the fixed image. In the mass preserving registration, the moving image is being deformed and interpolated after every level of the transform. Shrinkage of the moving image results in the increase of the density of lung parenchyma thus making lung parenchyma less distinguishable from the vessels. In the opposite case, the moving image is expanded and intensity of lung parenchyma decreases potentially leading to a more accurate alignment of vessels.

In 19 out of 20 cases, the proposed method produced invertible deformations. In the remaining case only for negligible percentage of voxels 0.01 % singularities occurred. Since we did not include the regularizer as a part of the cost function, we can conclude that with the multi-level transform strategy and the current setup of the optimization procedure we almost achieved invertibility of the transformation.

Overall mass preserving registration achieved an average landmark alignment score of 2.19 ± 2.05 mm and the median was 1.29 mm. The average ranking for this score was 22.15 was larger than average ranking for the remaining scores, ranging from 13.28 to 19.03. One of the reasons for large landmark alignment score could be in a large B-Spline grid, the average size of the B-Spline grid at the final transform level was $2.4 \times 1.8 \times 2.3$ cm^3. Although it could be further improved by applying additional levels of B-Spline transform with smaller grid size, it will also lead to the increase of the complexity of the image registration algorithm. In all the 5 cases, where the average landmark alignment score was above 5 mm, optimization procedure was stopped because of the maximum number of

iterations 1000 was reached. This could be improved by increasing the number of maximum iterations.

Figure 1 shows weak trend between the rank of the mass preserving registration algorithm and the relative lung volume difference for the fissure alignment and singularity scores. For the scan pairs with large lung volume difference, the proposed image registration method was generally ranked higher.

The mass preserving registration method was ranked 20th out of 34 participants. Consider the fact that number of degrees of freedom in transformation function was relatively small, we conclude that our registration algorithm was able to capture lung deformations with a relatively simple deformation model with acceptable spatial accuracy of 2.19 mm.

Acknowledgements This work is financially supported by the Danish Council for Strategic Research under the Programme Commission for Nanoscience and Technology, Biotechnology and IT (NABIIT), the Netherlands Organization for Scientific Research (NWO), and AstraZeneca, Lund, Sweden.

References

1. Sluimer, I., Schilham, A., Prokop, M., van Ginneken., B.: Computer analysis of computed tomography scans of the lung: A survey. IEEE Trans. on Med. Imag. **25** (2006) 385–405
2. Shaker, S.B., Dirksen, A., Laursen, L.C., Skovgaard, L.T., Holstein-Rathlou, N.H.: Volume adjustment of lung density by computed tomography scans in patients with emphysema. Acta Radiologica **4** (2004)
3. Sarrut, D., Boldea, V., Miguet, S., Ginestet, C.: Simulation of 4D-CT Images from Deformable Registration between Inhale and Exhale Breath-hold CT Scans. Med. Phys. **33**(3) (March 2006) 605–617
4. Simon, B.: Non-invasive imaging of regional lung function using X-ray computed tomography. Journal of Clinical Monitoring and Computing **16** (2000) 433–442
5. Reinhardt, J.M., Ding, K., Cao, K., Christensen, G.E., Hoffman, E.A., Bodas, S.V.: Registration-based estimates of local lung tissue expansion compared to xenon CT measures of specific ventilation. Med. Image Anal. **12**(6) (Dec 2008) 752–763
6. Zhu, L., Yang, Y., Haker, S., Tannenbaum, A.: An image morphing technique based on optimal mass preserving mapping. IEEE Trans. on Image Proc. **16** (2007) 1481–1495
7. Castillo, E., Castillo, R., Zhang, Y., Guerrero, T.: Compressible image registration for thoracic computed tomography images. Journal of Medical and Biological Engineering **29** (2009) 236–247
8. Gorbunova, V., Lo, P., Ashraf, H., Dirksen, A., Nielsen, M., de Bruijne, M.: Weight preserving image registration for monitoring disease progression in lung CT. In Metaxas, D., Axel, L., Székely, G., Fichtinger, G., eds.: Proc. Medical Image Computing and Computer Assisted Intervention (MICCAI). Volume 5242 of Lecture Notes in Computer Science. (2008) 863–870
9. Gorbunova, V., Lo, P., Loeve, M., Tiddens, H., Sporring, J., Nielsen, M., de Bruijne, M.: Mass preserving registration for lung CT. In Pluim, J., Dawant, B., eds.: SPIE (Medical Imaging). Volume 7259 of Proc. SPIE. (Feb 2009)
10. Yin, Y., Hoffman, E., Lin, C.L.: Local tissue-weight-based nonrigid registration of lung images with application to regional ventilation. In Pluim, J., Dawant, B., eds.: SPIE (Medical Imaging). Volume 7262 of Proc. SPIE. (2009)

11. Yin, Y., Hoffman, E.A., Lin, C.L.: Mass preserving nonrigid registration of CT lung images using cubic B-spline. Med. Phys. **36(9)** (2009) 4213–4222
12. Rueckert, D., Sonoda, L.I., Hayes, C., Hill, D.L.G., Leach, M.O., Hawkes, D.J.: Nonrigid registration using free-form deformations: Application to breast MR images. IEEE Trans. on Med. Imag. **18** (1999) 712–722
13. Mattes, D., Haynor, D., Vesselle, H., Lewellen, T., Eubank, W.: PET-CT image registration in the chest using free-form deformations. IEEE Trans. on Med. Imag. **22** (2003) 120–128
14. Lo, P., Sporring, J., Ashraf, H., Pedersen, J.J., de Bruijne, M.: Vessel-guided airway tree segmentation: A voxel classification approach. Medical Image Analysis **14**(4) (2010) 527 – 538
15. Murphy, K., van Ginneken, B., Pluim, J., Klein, S., Staring, M.: Semi-automatic reference standard construction for quantitative evaluation of lung CT registration. In Metaxas, D., Axel, L., Székely, G., Fichtinger, G., eds.: Proc. Medical Image Computing and Computer Assisted Intervention (MICCAI). Volume 5242 of Lecture Notes in Computer Science. (2008) 1006–1013
16. Wu, Z., Rietzel, E., Boldea, V., Sarrut, D., Sharp, G.C.: Evaluation of deformable registration of patient lung 4DCT with subanatomical region segmentations. Med. Phys. **35**(2) (Feb 2008) 775–781
17. Lo, P., Sporring, J., Ashraf, H., Pedersen, J., de Bruijne, M.: Vessel-guided airway segmentation based on voxel classification. In: First International Workshop on Pulmonary Image Analysis. (2008)
18. Rueckert, D., Aljabar, P., Heckemann, R.A., Hajnal, J.V., Hammers, A.: Diffeomorphic registration using b-splines. In Larsen, R., Nielsen, M., Sporring, J., eds.: Medical Image Computing and Computer Assisted Intervention. Volume 2. (2006) 702–709
19. Klein, S., Staring, M., Pluim, J.P.W.: Evaluation of optimization methods for nonrigid medical image registration using mutual information and B-splines. IEEE Trans. Image Process. **16**(12) (Dec 2007) 2879–2890
20. Hub, M., Kessler, M.L., Karger, C.P.: A stochastic approach to estimate the uncertainty involved in b-spline image registration. IEEE Trans. on Med. Imag. **28** (2009) 1708 – 1716
21. Schlathlter, T., Lorenz, C., Carlsen, I., Renisch, S., Deschamps, T.: Simultaneous segmentation and tree reconstruction of the airways for virtual bronchoscopy. In: Medical Imaging: Image Processing. Volume 4684 of SPIE. (2002) 103–113